An F-actin shell ruptures the nuclear envelope by sorting pore-dense and pore-free membranes in meiosis of starfish oocytes

Natalia Wesolowska[1], Pedro Machado[2], Celina Geiss[1], Hiroshi Kondo[1,3], Masashi Mori[1,4], Yannick Schwab[1,2], Péter Lénárt[1,5,6]

[1]Cell Biology and Biophysics Unit and [2]Electron Microscopy Core Facility, European Molecular Biology Laboratory (EMBL), Meyerhofstrasse 1, 69117 Heidelberg, Germany

[3]Present address: The Francis Crick Institute, London NW1 1AT, UK

[4]Present address: RIKEN Center for Developmental Biology, Minatojima-minamimachi, Chuo-ku, Kobe, Hyogo, 650-0047 Japan

[5]Present address: Max Planck Institute for Biophysical Chemistry, 37077 Göttingen, Germany

[6]Correspondence to: plenart@mpibpc.mpg.de

Abstract

In metazoa, the nuclear envelope (NE), composed of nuclear membranes, pores (NPCs) and the underlying network of lamin filaments, disassembles and reassembles in every division. A phase of sudden rupture is a conserved feature of NE breakdown (NEBD), a key cell-cycle event essential for timely spindle assembly and faithful chromosome segregation. This rupture involves mechanical forces generated by microtubules in somatic cells, and by the actin cytoskeleton in starfish oocytes. How cytoskeletal forces disrupt the NE remained unknown. Here, by live-cell and super-resolution light microscopy we show that at NEBD a transient cortex-like F-actin structure assembles within the lamina. This F-actin shell sprouts filopodia-like protrusions forcing apart the lamina and nuclear membranes. By correlated light and electron microscopy, we visualize that these F-actin spikes protrude pore-free nuclear membranes, while adjoining stretches accumulate packed NPCs. These NPC conglomerates sort into distinct membrane tubules and vesicles, while breaks appear in pore-free regions. We propose that the F-actin shell destabilizes the NE by forcing apart the lamina and nuclear membranes, providing the first mechanistic explanation for the sudden collapse of the NE during its breakdown.

Introduction

The nuclear envelope (NE), composed of inner and outer nuclear membranes, is a specialized sub-compartment of the endoplasmic reticulum (ER) separating nucleus and cytoplasm in eukaryotic cells. In metazoa, these membranes are supported by a network of intermediate filaments, the lamina, lining the nucleoplasmic side and providing mechanical stability to the NE (Burke and Ellenberg, 2002). The inner and outer NE is fused at nuclear pore complexes (NPCs) to create passageways to mediate nucleo-cytoplasmic transport.

Nucleocytoplasmic compartmentalization allows for sophisticated regulation of gene expression. However, this comes at a price: microtubule cytoskeleton, which is used by metazoa to segregate chromosomes in cell division, is strictly cytoplasmic. Therefore, the NE needs to be dismantled at the onset of every division to give microtubules access to chromosomes in the nucleus, and then reassembled at the end of division once the chromosomes are segregated. In deuterostomes, which include vertebrates as well as the echinoderm starfish, the complex NE structure is fully disassembled in a so-called 'open' division. This involves the disassembly of the NPCs, the depolymerization of the lamina, and re-absorption of the nuclear membranes into the ER (Hetzer, 2010; Ungricht and Kutay, 2017).

In all species where open NEBD has been investigated in detail, including mammalian somatic cells and oocytes of various species, NEBD has been found to proceed in two clearly discernible steps (Dultz et al., 2008; Mühlhäusser and Kutay, 2007; Terasaki et al., 2001; Lénárt et al., 2003). The first phase lasts 5-10 minutes during prophase and leads to a gradual and partial permeabilization of the NE due to phosphorylation-driven disassembly of the NPCs and other NE components (Linder et al., 2017; Martino et al., 2017). This allows proteins and complexes up to approx. 70 kDa (e.g. tubulin monomers) to leak in or out of the nucleus (Lénárt et al., 2003). Furthermore, it is likely that the mechanical properties of the NE are affected, i.e. the NE is weakened and destabilized as a result of phosphorylation of lamins and lamina-associated proteins (Ungricht and Kutay, 2017). Importantly however, during this first phase the overall structure of the NE, as seen for example by electron microscopy (EM), is still intact, and compartmentalization of large protein complexes (e.g. ribosomes, microtubules) is maintained (Terasaki et al., 2001; Lénárt et al., 2003).

The slow phosphorylation-driven weakening of the NE is followed by a sudden rupture of the NE in the second phase of NEBD, what leads to rapid and complete mixing of cyto- and nucleoplasm. As this dramatic change is easily visible even by transmitted light microscopy, this second step is commonly identified as 'NEBD,' marking the transition between prophase and prometaphase of cell division. Observations from several cell types suggest that this sudden rupture requires mechanical force generated by the cytoskeleton. Most prominently, in cultured mammalian cells microtubules have been shown to tear the NE in a dynein-dependent process, allowing for their timely access to chromosomes (Beaudouin et al., 2002; Salina et al., 2002).

As we and others have demonstrated earlier, starfish oocytes are an exceptionally well suited model to study open NEBD, as NEBD commences very reproducibly 20 min following hormonal induction of meiotic maturation. Furthermore, while the oocyte is still sufficiently transparent to allow high-resolution live-cell imaging, the very large 70-µm-diameter nucleus allows visualization of the process to an exceptional detail (Terasaki et al., 2001; Lénárt et al., 2003). Intriguingly, we have shown recently that in this exceptionally large oocyte nucleus, the actin rather than microtubule cytoskeleton is involved in the sudden rupture of the NE in the second phase of NEBD. A transient F-actin 'shell' is polymerized by the Arp2/3 complex on the inner surface of the NE and upon its passage, within less than two minutes, membranes undergo complete rupture (Mori et al., 2014). However, how the F-actin shell mediates this rapid and dramatic reorganization of the NE, remained unknown.

Here, we use a combination of live-cell and super-resolution light microscopy, and correlated electron microscopy to capture these sudden changes in NE organization. We find that the F-actin shell is nucleated within the still-intact lamina and projects filopodia-like spikes into the nuclear membranes. The resulting nuclear membrane protrusions are free of NPCs, and are juxtaposed by valleys, in which

NPCs cluster. Subsequently, these NPC conglomerates invaginate and sort into NPC-rich membrane vesicles and tubules, while breaks appear on the pore-free regions. Thus, we propose that the F-actin shell generates force by actin polymerization and wrestles apart the nuclear membranes and the underlying lamina. This destabilizes the NE by segregation of NPC-containing membranes still associated with the lamina from pore-free nuclear membranes.

Results

The F-actin shell appears in a stereotypic pattern allowing to track progress of NE rupture

We have shown previously that the F-actin shell is required for the sudden breakdown of the NE (Mori et al., 2014). However, our previous live-cell imaging assays lacked the resolution to visualize structural details of this dramatic reorganization occurring at the sub-micrometer scale. Therefore, we optimized staining and imaging protocols, and we developed an antibody against the only identified starfish lamin protein (see Materials and Methods for details). This, together with the pan-NPC antibody mAb414 enabled us to co-visualize endogenous NE components with phalloidin for F-actin at high resolution.

As we have shown previously, the F-actin shell is very transient, polymerizing and depolymerizing again within 2 minutes, necessitating a reliable temporal reference for fixed-cell assays. Fortunately, the F-actin shell emerges in a highly reproducible spatial pattern, which enabled us to precisely time fixed samples by correlating them with morphologies observed in live cell recordings (compare Fig. 1A and B). At the earliest stages, when the NE is still intact and impermeable to large dextrans, the F-actin shell appears on the inner side of NE as an equatorial band composed of F-actin foci (Fig. 1A, 0 s). Then, as these F-actin foci grow and intensify, merging into a continuous F-actin shell, the first breaks on the NE appear, visualized by localized entry of large dextrans (Fig. 1A, 45 s). Thereafter, the shell spreads, followed by a wave of membrane breakdown with an approx. 30 s delay (Mori et al., 2014). By the time breakdown reaches across the whole nuclear surface, the F-actin shell disassembles in the equatorial region, where it first appeared (Fig. 1A, 90 s).

Using these distinct morphological features of the dynamically assembling and disassembling F-actin shell, we were able to reliably identify and order the progress of NE rupture in fixed samples.

The overall structure of the lamina remains intact during F-actin-driven NE rupture

Next we wanted to clarify whether the F-actin shell destabilizes the NE by tearing the lamin network, as it has been reported in somatic cells for microtubule-driven NE rupture (Beaudouin et al., 2002; Salina et al., 2002). We have addressed this question earlier in starfish oocytes, however, at that time we exogenously overexpressed a GFP fusion of human lamin B, which could have had different disassembly kinetics (Lénárt et al., 2003).

We therefore carefully analyzed samples stained with the starfish anti-lamin antibody at different stages of NE rupture, timed by the F-actin staining pattern, as described above. This confirmed our previous observations that even minutes after NE rupture the endogenous lamin network remains continuous at the resolution of the light microscope, although it folds and ruffles as the nucleus collapses during NEBD (Fig. 1C).

Thus, we conclude that the rupture the NE does not proceed by F-actin-induced tearing or rapid disassembly of the lamina.

F-actin shell assembles within the lamina sprouting spikes that push to detach nuclear membranes

We next co-localized the lamina or the nuclear membranes (as marked by NPCs) together with the F-actin shell, stained by phalloidin. We observed that while the NPC staining clearly formed a separate layer ‘above’ the F-actin shell, the lamina co-localized with phalloidin labeling (Fig. 2A, B). This is

confirmed by line profiles across the NE, revealing an approx. 500 nm separation between NPC and F-actin staining at the time of NE rupture, as opposed to the tight co-localization observed with lamina (Fig. 2A, B). Thus, the still-intact lamina appears to serve as the scaffold upon which the F-actin shell assembles, whereas the nuclear membranes separate and seem to detach from the lamina by the forming F-actin shell.

Closer investigation of these samples revealed F-actin spikes extending from the base of the F-actin shell towards and through nuclear membranes (Fig 2C). Indeed, at high resolution the NPC signal showed a fragmented appearance with F-actin spikes coming out through gaps in NPC array (Fig. 2C). Surface views revealed that these NPC fragments form a complex network on the surface of the nucleus (Fig. 2C).

These images are very suggestive of spikes pushing or even piercing the NE. In an attempt to visualize fine details of this process, we turned to stimulated emission depletion (STED) microscopy, which is a superresolution technique compatible with our thick, whole-mount samples. However, unfortunately, our staining protocol was incompatible with co-labeling F-actin by phalloidin and NE by antibodies for STED, thus we imaged them separately.

Phalloidin labeling of the F-actin shell revealed a dense array of filopodia-like F-actin spikes of 0.5-2 µm in length spaced approx. 0.1 µm, and protruding from the base of the F-actin shell towards the nuclear membranes (Fig. 2D). This is consistent with our above and earlier observations by confocal microscopy (Mori et al., 2014), however due to the lower resolution of the confocal microscope, earlier we largely underestimated the number of spikes and were unable to resolve their morphology.

We next used antibody staining of NPCs and lamina to visualize NE structure at the resolution of STED (these samples were also stained with phalloidin used for staging, not shown). Before NE rupture, the NPC staining and lamina overlapped, even at the approx. 50 nm resolution afforded by STED (Fig. 2E, pre-NEBD). This is consistent with the known ultrastructure of the NE with the lamina being tightly associated with the nuclear membranes (Burke and Ellenberg, 2002).

In stark contrast to the interphase situation, at the time of F-actin shell formation we could visualize NPC-stained NE fragments “floating” above the intact lamina (Fig 2E, post-NEBD), consistent with confocal images. This detachment is dependent on the F-actin shell, because when we prevented F-actin shell formation by inhibiting the Arp2/3 actin nucleator complex by the small molecule inhibitor, CK-666, lamina and NPCs did not separate (Fig. 2E, post-NEBD + CK-666). (Note: in CK-666 samples NPC and lamin staining weakens due to the continuing disassembly of NE components, whereas the nucleus collapses as a result of the progressing permeabilization (Mori et al., 2014)). This is consistent with our earlier findings showing that F-actin-driven NE rupture is Arp2/3 dependent (Mori et al., 2014), and suggests that detachment of the NPCs from the lamina is a key step of this process.

Taken together, light microscopy of the F-actin shell and NE components reveals that the F-actin shell nucleates in the lamina and extends filopodia-like spikes towards the nuclear membranes. In this process the nuclear membranes detach from the lamina and rearrange to an NPC-dense reticular network on the nuclear surface. However, a critical issue in interpreting these results is that we rely on the NPC staining to represent nuclear membranes. As the oocyte NE in interphase is fully packed with an almost crystalline array of NPCs (Lénárt et al., 2003), the assumption is reasonable, but during NE rupture exactly this arrangement may change. Unfortunately, our efforts to visualize the nuclear membranes by light microscopy remained futile, because preserving F-actin requires addition of detergents to the fixative, which is incompatible with preserving fine membranous structures. Thus, we turned to correlated light and electron microscopy.

Correlative EM captures intermediates of NE rupture

In order to clarify the F-actin mediated rearrangements of the nuclear membranes, we wanted to target its early stages, the approx. 30 s time-window when parts of the NE are already ruptured, while other regions are still intact. We expected that at this stage we could observe intermediate steps of

NE rupture, spatially arranged within the same sample. The challenge was to immobilize oocytes at this exact time of F-actin shell formation.

For this purpose we developed a correlative electron microscopy protocol using high-pressure freezing and freeze substitution resulting in an excellent preservation of cellular structures (see Materials and Methods and Burdyniuk et al., 2018). Correlation to light microscopy was possible thanks to the fact that the protocol preserves fluorescence in EM sections. In order to avoid any potential artifacts caused by direct labeling of F-actin or NE components, we used fluorescently-labeled dextrans as indicators of NEBD progression: a small, 25 kDa dextran enters the nucleus already in the first phase of NEBD through the disassembling NPCs, while the large, 160 kDa dextran only enters when the NE is ruptured (Lénárt et al., 2003). Thus, as shown in the live-cell time-series, with labeling for both dextrans as well as for F-actin, the moment when the small, 25 kDa dextran almost completely fills the nucleus, but the large, 160 kDa dextran is still excluded corresponds to the time-window when F-actin shell forms and NE ruptures (Fig. 3A).

Accordingly, we froze the samples blind at the approximate time of NEBD, and screened by light microscopy on EM sections for the stage, when the small dextran already filled the nucleus, but the large dextran was still excluded (Fig. 3B). We then performed automated large field of view montage transmission EM imaging of the whole nuclear cross-section to assess the state of the nuclear envelope. An overview is shown in Fig. 3C, this and two additional montages are available at high resolution as Supplemental Data (Fig. S1-3). The montage illustrates the key advantage of our model system, whereby the progression of NE rupture can be observed spatially ordered on a single section of the large oocyte nucleus. The arrangement of the rupture site is fully consistent with live and fixed light microscopy data: NE rupture initiates near the 'equator' of the nucleus spreading as a wave towards the poles (Fig. 3D).

We carefully examined these large montages and observed a set of frequently reoccurring characteristic membrane configurations during the progression of NE rupture. We defined them into four categories and assigned each a symbol in order to mark their incidence on the montage (Fig. 3C). Numbers in Fig. 3D under each category quantify the occurrence of each feature within the section, and numbers in parentheses represent similar quantification in two other sections shown in the Supplement, illustrating that these are rather frequently occurring structures at the time of NE rupture.

Taken together, using our correlative light and electron microscopy approach, we were able to capture oocytes in the process of NE rupture. The spatial arrangement of breakdown intermediates precisely correlated with the expected spatio-temporal progression of NE rupture, as visualized in live and fixed cells (Fig. 3C).

F-actin spikes protrude pore-free nuclear membranes

The large dataset, the high frequency of events observed, and importantly the spatial arrangement from the equatorial rupture site towards the still-intact poles, allowed us to reconstruct the steps of NE rupture.

Consistent with earlier observations (Lénárt et al., 2003), in immature oocytes, as well as in oocytes just before NE rupture, and even in the intact, polar regions of an oocyte undergoing rupture, the NE is smooth, continuous and is tightly packed with NPCs with a regular spacing of approx. 200 nm (Fig. 4A, B and 5D). (Note: all micrographs are false-colored for cytoplasm and nucleus as judged by the presence or absence of ribosomes.)

In striking contrast, in areas closer to the rupture site we observed regions with gaps in NPC occupancy (Fig. 4C), the number and size of which increased towards the rupture site. Closer to the rupture site these gaps appeared to evolve into 'bumps' and membrane spikes (Fig. 4D). Although reconstructing the full 3D architecture of these spikes is challenging even in 300-nm-thick tomographic sections, the most prominent spikes we observed rise approx. 1 µm above the level of the NE, exactly matching in

size to F-actin spikes seen by phalloidin staining (Fig. 4D, E). These spikes contain fibrous densities matching in size and morphology with actin filaments (Inset 3, Fig. 4E), even clearer distinguishable on tomographic reconstructions (Fig. 4F). Importantly, both on thin sections and tomographic reconstructions we observed these spikes to be covered by continuous nuclear membranes almost completely free of NPCs. These pore-free areas are surrounded by NPC-dense adjacent regions.

While these data are fully consistent with immunofluorescence shown on previous figures, they also show that relying on NPC staining as a marker for nuclear membranes during NEBD is misleading. Our EM data reveals that F-actin spikes that were interpreted on immunofluorescent images to pierce nuclear membranes, are in fact covered by pore-free nuclear membranes. These data rather suggest that the growing gaps between NPCs, which then develop into bumps and spikes, are extruded by the F-actin shell. On a global scale the F-actin shell appears to sort the NE to pore-free and NPC-dense regions, while leaving the membrane boundary initially still intact.

NPC-rich membranes sort into a tubular-vesicular network while pore-free regions rupture

Striking and very surprising intermediates observed accompanying the spikes are the nucleoplasmic bodies: dense, round structures beneath the NE in the nucleoplasm (Fig. 4D, arrows). These bodies of approx. 200-500 nm in diameter are observed very frequently, and they often appear in a beads-on-a-string arrangement with a slightly electron-denser nucleoplasmic material connecting them (Fig. 5A, see also Fig. 3C and S1-3 for full datasets).

Upon careful examination and juxtaposition of intermediates, we were able to gain insights into how the nucleoplasmic bodies may form. First, in neighborhood of spikes and pore-free regions we often see NPC aggregates forming pits curving into the nucleoplasm (Fig. 5A, inset 1). Then, occasionally, we observed strongly curved dimples reminiscent of membrane vesiculation. Finally, we even identified membrane configurations apparently fused at the neck of the invagination (Fig. 5A, insets 2, 3). This suggests that nucleoplasmic bodies may be inverted NE tubules filled with cytoplasm inside (evidenced by the presence of ribosomes, Fig. 5A, inset 4). Tomograms also confirm that the electron density along the boundary of the bodies corresponds to closely juxtaposed NPCs with an intact central ring structure (Fig. 5B).

Intriguingly, even when nucleoplasmic bodies are seen deep in the nucleoplasm, above them the NE appears to be still intact, consisting mostly of NPC-free nuclear membranes and still maintaining the nucleo-cytoplasmic boundary as judged by the distribution of ribosomes (Fig. 5A). Only in areas where the nucleoplasmic bodies are most frequent and exaggerated, we observe membrane rupture evidenced by presence of ribosomes in the nuclear regions (Fig. 5C). In these areas nucleoplasmic bodies are neighbored by straight bits of NPC-packed membranes.

The exact mechanism of sorting into NPC aggregates and subsequent rupture remains unclear, however we observed that NPC density increases in ‘dimples’ (see more examples on Fig. S4) to almost double, approx. 100 nm on average, of that in the intact NE in immature oocytes or oocytes a few minutes before NEBD with a quite regular NPC spacing around 200 nm (Fig. 5D). The NPC density appears to increase gradually in the process of NE rupture with a broad distribution around 160 nm as gaps start appearing in the membrane, and decreasing down to 100 nm (Fig. 5D, S4). We are unable to estimate the 3D membrane areas from 2D sections, nevertheless these observations suggest that NPC-free areas pushed out by the F-actin shell may lead to crowding of NPCs in juxtaposed regions. It then appears that densely packed NPCs prefer a curved membrane configuration leading ‘dimpling’ and eventual invagination.

Model for F-actin-driven nuclear envelope rupture

Here, we resolved structural intermediates of rapid NE rearrangements mediated by the transient F-actin shell by using immunostaining and correlative EM in starfish oocytes. Based on these data we propose the following model for NE rupture (Fig. 6). The first step is formation of F-actin foci within

the lamina. We hypothesize that these foci form at the time when cytoplasmic components, such as the Arp2/3 complex and actin monomers, reach a critical concentration in the nucleus, as a result of the gradual, phosphorylation-driven disassembly and increasing leakiness of the NPCs in the first phase of NEBD. Once triggered, F-actin foci grow rapidly, which is expected based on the autocatalytic nature of Arp2/3-mediated nucleation of branched F-actin networks. As they spread, they start to form a continuous shell. The filaments seem to preferentially grow from the shell base in the lamina towards nuclear membranes, and push against them. This asymmetry may be explained by fact that force imposed on actin filaments promotes nucleation of branched meshwork (Bieling et al., 2016). Intriguingly, F-actin networks nucleated *in vitro* on micropatterned activated Arp2/3 show a strikingly similar morphology to the F-actin shell with filopodia-like bundles pointing away from a base of dense branched network (Reymann et al., 2010). This strongly suggests that localized activation of Arp2/3 within the lamina may be sufficient to explain the morphology of the F-actin shell.

Our EM data clearly show that the F-actin shell protrudes pore-free nuclear membranes, separating these from the lamina. We hypothesize that these membranes are cleared of NPCs, because NPCs may still attach to the lamina at this stage, and thus are held back, while membranes are pushed out by the F-actin shell. Then, as the NPCs accumulate in the NE dimples between pore-free spikes, membranes buckle into the nucleoplasm and invaginate to form nucleoplasmic bodies. Our data suggest that pore-free nuclear membranes separated from the lamina are unstable, and thus rupture and rearrange into an ER-like reticular structure.

In agreement with our model, it has been shown in various other physiological contexts that weakening the lamin network leads to NE rupture. For example, NE rupture frequently occurs in cancer cells, in particular in micronuclei, where breaching of the NE barrier is preceded by local lamin disruption (Hatch et al., 2013). More generally, recent work shows that the "breakability" of the nucleus in migrating cells is dependent on lamin composition (Thiam et al., 2016; Davidson and Lammerding, 2014; Denais et al., 2016). Additionally, recent work revealed that repair of interphase NE rupture, as well as reassembly of NE after division, involves the ESCRT machinery (Denais et al., 2016; Raab et al., 2016; Olmos et al., 2015). In our NEBD intermediates we observe similar membrane topologies to those involved in NE repair, suggesting that the ESCRT complex may also be recruited to NE invaginations and may play a role in forming the reticular network of nucleoplasmic bodies.

Finally, the clearing of NPCs off the membrane appears to be conserved to NEBD in organisms with partially open mitosis. Tearing of the NE has been observed in the fungus *Ustilago maydis* and the yeast *Schizosaccharomyces japonicus*. In *U. maydis* the shearing is caused by microtubules pulling the nucleus through a small opening into the bud of the daughter cell (Straube et al., 2005). *Sz. japonicus,* on the other hand, splits the NE by stretching the nucleus between the two poles of a dividing cell (Aoki et al., 2011). Thus, NE rupture occurs by different means, but intriguingly both show evidence of clearing NPCs before the NE is torn: *Sz. japonicus* redistributes the NPCs to the two poles freeing naked membranes at the NE regions destined to be broken. NPCs of *U. maydis* on the other hand initiate release of nucleoporins prior to rupture just as higher eurkaryotes (Straube et al., 2005; Aoki et al., 2011; Theisen et al., 2008).

Taken together, our data suggest that the F-actin shell destabilizes the NE by forcing apart the lamina and nuclear membranes, providing the first mechanistic explanation for the sudden collapse of the NE structure during its breakdown that may be related in mechanism to nuclear rupture frequently observed in cancer cells.

Materials and methods

Oocyte collection and injection

Starfish (*Patiria miniata*) were obtained in the springtime from Southern California (South Coast Bio-Marine LLC, Monterey Abalone Company or Marinus Scientific Inc.) and kept at 16°C for the rest of the year in seawater aquariums of EMBL's marine facilities. Oocytes were extracted from the animals fresh for each experiment as described earlier (Lénárt et al., 2003). mRNAs and other fluorescent markers were injected using microneedles, as described previously (Jaffe and Terasaki, 2004; Borrego-Pinto et al., 2016). mRNA was injected the day before to allow protein expression, while fluorescently labeled protein markers or dextrans were injected a few hours prior to imaging. Meiosis was induced at initiation of experiment by addition of 1-methyladenine (1-MA, 10 µM, Acros Organics). NEBD normally started at 20-25 minutes after 1-MA addition.

Fluorescent markers and antibodies

To label F-actin, UtrCH-3mEGFP mRNA was synthesized *in vitro* from linearized DNA templates using the AmpliCap-Max T7 High Yield Message Maker kit (Cellscript), followed by polyA-tail elongation (A-Plus Poly(A) Polymerase Tailing Kit, Cellscript). mRNAs were dissolved in water (typical concentration 3-5 µg/µl) and injected into the oocyte up to 5% of the oocyte volume.

Phalloidin labeled with the indicated Alexa fluorophores (Invitrogen) was dissolved in methanol, and was then air-dried prior to use and dissolved in PBS for immunostaining.

For dextrans, amino-dextrans were labeled with succinimidyl ester dye derivatives (Cy5) or purchased already in labeled form (TRITC), purified and injected into oocytes as described earlier (Lénárt et al., 2003).

The pan-NPC antibody mAb414 was purchased from BioLegend (catalogue #902907). To produce the anti-starfish-lamin antibody, first the *Patiria miniata* lamin sequence identified by BLAST searches in our transcriptome-based database (http://www.lenartlab.embl.de:4567/) by comparisons to the human lamin B amino acid sequence, and confirmed by reverse searches to other species. Furthermore, the corresponding mRNA was expressed as a mEGFP fusion and showed the expected localization to the NE in starfish oocytes (not shown). Peptide antibodies were then produced against the "histone-interaction peptide" region of starfish lamin (GTKRRRLDEEESMVQSS), which was used as the antigen for rabbit immunization. Antibody production and affinity purification was performed by Cambridge Research Biochemicals. The antibody's specificity was confirmed in Western blot showing an expected-sized band and immunostaining showing localization to the nuclear rim in starfish oocytes.

Immunostaining

Oocytes were fixed at desired times in a PFA/GA fixative (100 mM HEPES pH 7.0, 50 mM EGTA, 10 mM $MgSO_4$, 0.5% Triton-X100, 1% formaldehyde, 0.4% glutaraldehyde) modified from Strickland et al. (Strickland et al., 2004). Active aldehyde groups remaining post fixation were quenched by 0.1% solution of $NaBH_4$. Subsequently, samples were permeabilized and blocked in PBS+0.1% Triton-X100 plus the Image-IT reagent (ThermoFisher Scientific). Antibody staining was done overnight for the primary antibody and for 2 h for the secondary antibody in PBS+0.1% Triton-X100. Oocytes were mounted with the antifade agent ProLongGold (ThermoFisher Scientific) under a coverslip pressed quite firmly onto tiny pillars of grease.

Light microscopy

Live cell movies were acquired on a Leica SP5 confocal microscope using a 40x HCX PL AP 1.10 NA water immersion objective lens (Leica Microsystems). Fixed oocytes were imaged on a Leica SP8

microscope equipped with the HC PL APO 1.40 NA 100x oil immersion objective according to Nyquist criteria. For STED imaging, suitable Abberior STAR 580 and Abberior STAR RED secondary antibodies were used (Abberior GmbH). Samples were imaged on a Leica SP8 STED microscope, with the HC PL APO CS2 1.40 NA 100x oil immersion objective and using 570 nm laser for Abberior STAR 580 and 633 nm for Abberior STAR RED and the 775 nm depletion laser.

Images were deconvolved using the Huygens software (Scientific Volume Imaging) with either confocal or STED settings as appropriate.

Electron microscopy

The protocol is described in detail in Burdyniuk et al. (Burdyniuk et al., 2018). In brief, oocytes were injected with a mixture of dextrans and a small batch was tested for meiosis timing. At the approximate time of NEBD they were transferred into a carrier (3 oocytes in 0.3 µl of sea water) and most of the water was removed with filter paper. Oocytes were immediately covered with a drop of 1-hexedecene, and immediately high-pressure frozen. Oocytes were freeze-substituted into Lowicryl HM-20. To stage the oocytes, light microscopy of EM sections was used to determine the progress of dextran entry. Selected sections were then post-stained with lead citrate and imaged using a BioTwin CM120 Philips transmission electron microscope at 120 kV. Large TEM montages were acquired using a JEOL JEM-2100Plus transmission electron microscope at 120 kV. Tomograms were reconstructed from tilt series acquired on FEi Tecnai F30 transmission electron microscope at 300 kV with 1.554 nm pixel size.

Acknowledgements

We thank the members of the Lénárt laboratory for reagents and support, in particular Kálmán Somogyi, Andrea Callegari, Johanna Bischof, Joana Borrego-Pinto and Philippe Bun. We also thank EMBL's Advanced Light Microscopy Facility for essential support, specifically Marko Lampe for the help with STED imaging. We thank the Electron Microscopy Core Facility, and Paolo Ronchi for sharing expertise during development of the EM protocol. We thank EMBL's Laboratory Animal Resources and Kresimir Crnokic in particular.

Research in P.L.'s laboratory is funded by the European Molecular Biology Laboratory (EMBL) and the Deutsche Forschungsgemeinschaft (DFG) through the grant GZ LE 2926/1-1 AOBJ 603520 in frames of the Priority Programme SPP 1464.

Competing interests: The authors declare no competing financial interests.

Author contributions: N.W. and P.L. conceived the project and designed the experiments. N.W. performed most experiments, H.K. and M.M. provided additional experimental data, and C.G. analyzed tomograms. N.W. and P.M. carried out electron microscopy under supervision of Y.S. N.W. and P.L. wrote the manuscript.

References

Aoki, K., H. Hayashi, K. Furuya, M. Sato, T. Takagi, M. Osumi, A. Kimura, and H. Niki. 2011. Breakage of the nuclear envelope by an extending mitotic nucleus occurs during anaphase in Schizosaccharomyces japonicus. *Genes Cells Devoted Mol. Cell. Mech.* 16:911–926. doi:10.1111/j.1365-2443.2011.01540.x.

Beaudouin, J., D. Gerlich, N. Daigle, R. Eils, and J. Ellenberg. 2002. Nuclear envelope breakdown proceeds by microtubule-induced tearing of the lamina. *Cell*. 108:83–96.

Bieling, P., T.-D. Li, J. Weichsel, R. McGorty, P. Jreij, B. Huang, D.A. Fletcher, and R.D. Mullins. 2016. Force Feedback Controls Motor Activity and Mechanical Properties of Self-Assembling Branched Actin Networks. *Cell*. 164:115–127. doi:10.1016/j.cell.2015.11.057.

Borrego-Pinto, J., K. Somogyi, and P. Lénárt. 2016. Live Imaging of Centriole Dynamics by Fluorescently Tagged Proteins in Starfish Oocyte Meiosis. *In* Methods in molecular biology (Clifton, N.J.). 145–166.

Burdyniuk, M., N. Wesolowska, M. Fleszar, M.A. Karreman, P. Machado, J. Borrego-Pinto, B. Ruthensteiner, Y. Schwab, and P. Lénárt. 2018. Correlated light and electron microscopy of cell division in large marine oocytes, eggs, and embryos. *Methods Cell Biol.* 145:293–313. doi:10.1016/bs.mcb.2018.03.031.

Burke, B., and J. Ellenberg. 2002. Remodelling the walls of the nucleus. *Nat. Rev. Mol. Cell Biol.* 3:487–497. doi:10.1038/nrm860.

Davidson, P.M., and J. Lammerding. 2014. Broken nuclei--lamins, nuclear mechanics, and disease. *Trends Cell Biol.* 24:247–256. doi:10.1016/j.tcb.2013.11.004.

Denais, C.M., R.M. Gilbert, P. Isermann, A.L. McGregor, M. te Lindert, B. Weigelin, P.M. Davidson, P. Friedl, K. Wolf, and J. Lammerding. 2016. Nuclear envelope rupture and repair during cancer cell migration. *Science*. 352:353–358. doi:10.1126/science.aad7297.

Dultz, E., E. Zanin, C. Wurzenberger, M. Braun, G. Rabut, L. Sironi, and J. Ellenberg. 2008. Systematic kinetic analysis of mitotic dis- and reassembly of the nuclear pore in living cells. *J. Cell Biol.* 180:857–865. doi:10.1083/jcb.200707026.

Hatch, E.M., A.H. Fischer, T.J. Deerinck, and M.W. Hetzer. 2013. Catastrophic nuclear envelope collapse in cancer cell micronuclei. *Cell*. 154:47–60. doi:10.1016/j.cell.2013.06.007.

Hetzer, M.W. 2010. The nuclear envelope. *Cold Spring Harb. Perspect. Biol.* 2:a000539. doi:10.1101/cshperspect.a000539.

Jaffe, L.A., and M. Terasaki. 2004. Quantitative microinjection of oocytes, eggs, and embryos. *Methods Cell Biol.* 74:219–42.

Lénárt, P., G. Rabut, N. Daigle, A.R. Hand, M. Terasaki, and J. Ellenberg. 2003. Nuclear envelope breakdown in starfish oocytes proceeds by partial NPC disassembly followed by a rapidly spreading fenestration of nuclear membranes. *J. Cell Biol.* 160:1055–1068. doi:10.1083/jcb.200211076.

Linder, M.I., M. Köhler, P. Boersema, M. Weberruss, C. Wandke, J. Marino, C. Ashiono, P. Picotti, W. Antonin, and U. Kutay. 2017. Mitotic Disassembly of Nuclear Pore Complexes Involves CDK1- and PLK1-Mediated Phosphorylation of Key Interconnecting Nucleoporins. *Dev. Cell*. 43:141-156.e7. doi:10.1016/j.devcel.2017.08.020.

Martino, L., S. Morchoisne-Bolhy, D.K. Cheerambathur, L. Van Hove, J. Dumont, N. Joly, A. Desai, V. Doye, and L. Pintard. 2017. Channel Nucleoporins Recruit PLK-1 to Nuclear Pore Complexes to Direct Nuclear Envelope Breakdown in C. elegans. *Dev. Cell*. 43:157-171.e7. doi:10.1016/j.devcel.2017.09.019.

Mori, M., K. Somogyi, H. Kondo, N. Monnier, H.J. Falk, P. Machado, M. Bathe, F. Nédélec, and P. Lénárt. 2014. An Arp2/3 nucleated F-actin shell fragments nuclear membranes at nuclear

envelope breakdown in starfish oocytes. *Curr. Biol. CB*. 24:1421–1428. doi:10.1016/j.cub.2014.05.019.

Mühlhäusser, P., and U. Kutay. 2007. An in vitro nuclear disassembly system reveals a role for the RanGTPase system and microtubule-dependent steps in nuclear envelope breakdown. *J. Cell Biol.* 178:595–610. doi:10.1083/jcb.200703002.

Olmos, Y., L. Hodgson, J. Mantell, P. Verkade, and J.G. Carlton. 2015. ESCRT-III controls nuclear envelope reformation. *Nature*. 522:236–239. doi:10.1038/nature14503.

Raab, M., M. Gentili, H. de Belly, H.R. Thiam, P. Vargas, A.J. Jimenez, F. Lautenschlaeger, R. Voituriez, A.M. Lennon-Duménil, N. Manel, and M. Piel. 2016. ESCRT III repairs nuclear envelope ruptures during cell migration to limit DNA damage and cell death. *Science*. 352:359–362. doi:10.1126/science.aad7611.

Reymann, A.-C., J.-L. Martiel, T. Cambier, L. Blanchoin, R. Boujemaa-Paterski, and M. Théry. 2010. Nucleation geometry governs ordered actin networks structures. *Nat. Mater.* 9:827–832. doi:10.1038/nmat2855.

Salina, D., K. Bodoor, D. Eckley, T. Schroer, J.B. Rattner, and B. Burke. 2002. Cytoplasmic dynein as a facilitator of nuclear envelope breakdown. *Cell*. 108:97–107.

Straube, A., I. Weber, and G. Steinberg. 2005. A novel mechanism of nuclear envelope break-down in a fungus: nuclear migration strips off the envelope. *EMBO J.* 24:1674–1685. doi:10.1038/sj.emboj.7600644.

Strickland, L., G. von Dassow, J. Ellenberg, V. Foe, P. Lenart, and D. Burgess. 2004. Light microscopy of echinoderm embryos. *Methods Cell Biol.* 74:371–409.

Terasaki, M., P. Campagnola, M.M. Rolls, P.A. Stein, J. Ellenberg, B. Hinkle, and B. Slepchenko. 2001. A new model for nuclear envelope breakdown. *Mol. Biol. Cell*. 12:503–510.

Theisen, U., A. Straube, and G. Steinberg. 2008. Dynamic rearrangement of nucleoporins during fungal “open” mitosis. *Mol. Biol. Cell*. 19:1230–1240. doi:10.1091/mbc.e07-02-0130.

Thiam, H.-R., P. Vargas, N. Carpi, C.L. Crespo, M. Raab, E. Terriac, M.C. King, J. Jacobelli, A.S. Alberts, T. Stradal, A.-M. Lennon-Dumenil, and M. Piel. 2016. Perinuclear Arp2/3-driven actin polymerization enables nuclear deformation to facilitate cell migration through complex environments. *Nat. Commun.* 7:10997. doi:10.1038/ncomms10997.

Ungricht, R., and U. Kutay. 2017. Mechanisms and functions of nuclear envelope remodelling. *Nat. Rev. Mol. Cell Biol.* 18:229–245. doi:10.1038/nrm.2016.153.

Figure legends

Figure 1. The lamina remains intact during NE rupture shown in precisely staged fixed samples
(A) Live imaging of UtrCH-3mEGFP (white) and Dextran-500kDa (red) in a starfish oocyte undergoing NEBD. Selected single confocal sections are shown from a time series; scale bar is 20 µm. **(B)** Fixed samples with F-actin labeled by phalloidin-AlexaFluor568. Individual confocal sections are shown and ordered to match the live time series in (A). Scale bar is 20 µm. **(C)** Immunostained starfish oocytes with anti-lamin antibody shown in cyan and phalloidin-AlexaFluor568 in red. Shown are three time-points: early shell, full shell and post shell. Each panel shows a maximum projection of the whole z-stack (left), a single selected optical section at the equatorial plane (right), and a zoom of the area in the single section highlighted with dashed rectangle (bottom). The zoom only shows the lamin channel. Scale bars are 20 and 5 µm, respectively.

Figure 2. High resolution light microscopy resolves separation of lamina and nuclear membranes during NEBD
(A) Left: Portion of the NE undergoing rupture immunostained with mAb414 for NPCs (cyan) and phalloidin-AlexaFluor568 for F-actin (red). Shown is a crop of a portion of NE from a thin confocal Z-section; scale bar 2 µm. Right: Plot of a line profile over the region marked with a white rectangle; normalized intensities of both channels are shown. **(B)** Same as (A), except stained with anti-lamin antibody and phalloidin-AlexaFluor568. **(C)** Immunostaining of a portion of the NE undergoing NEBD by mAb414 (cyan) and phalloidin-AlexaFluor568 (red). Shown are selected regions from a single confocal Z-stack. Left: sections at z = 0 nm and z = 300 nm. Right shows an *en face* view of the NE. Scale bars: 2 µm. **(D)** Phalloidin-Alexa568 staining of F-actin shell imaged by STED microscopy. Two areas are shown: one close to the vegetal pole (left) and one closer to the animal pole rotated so that the spikes point up (right). Scale bars are 5 µm (left) and 2 µm (right and inset on left). **(E)** Portions of the NE stained with anti-lamin antibody (cyan) and mAb414 (red) and imaged by STED. Left: before NEBD, middle: after NEBD, right: after NEBD and treated with CK-666 to inhibit the formation of the F-actin shell. Insets show regions outlined by orange dashed rectangles. Scale bars are 2 µm and 500 nm (insets).

Figure 3. Correlative EM approach captures NEBD intermediates
(A) Live imaging of a starfish oocyte undergoing NEBD and injected with a 25 kDa Cy5-labeled dextran (cyan) 160 kDa TRITC-labeled dextran (red) and UtrCh-3mEGFP (white). Shown are selected 2-frame projections from a confocal time-series imaged at 1 frame per second. Orange line marks the moment right prior to rupture of the membrane, corresponding to the predicted time for the EM sample shown in (B) and (C). Scale bar is 20 µm. **(B)** Wide-field fluorescence image of a 70 nm section of a Lowicryl-embedded oocyte undergoing NEBD and injected with 25 kDa Cy5-labeled dextran (cyan) and 160 kDa TRITC-labeled (red) dextran. Scale bar is 20 µm. **(C)** A whole-nucleus tile of transmission EM images stitched automatically for another section from oocyte shown in B. Symbols around the nucleus correspond to different events of NE rupture membrane intermediates observed. The symbol legend with examples (crops from the tiled image) is shown to the right. Under each symbol, numbers correspond to the count of these events in the section shown, and in parentheses the count in two adjacent sections (shown in Fig. S2-3). The band tracing the NE within the nuclear space demarcates areas with color-code for predominant membrane features. For full resolution image, see Fig. S1. Scale bar is 10 µm. **(D)** An oocyte fixed and stained with anti-lamin antibody (cyan) and phalloidin-AlexaFluor568 timed for early shell formation. Shown is a maximal projection of a Z-stack through half the nucleus. Right: a scheme illustrating the 3D geometry of the EM section. Scale bar is 20 µm.

Figure 4. Spikes protrude bare nuclear membranes
(A-D) Transmission EM images from the oocyte shown in Fig. 3D showing intermediates of NE rupture. Transparency coloring distinguishes the cytoplasm (green) from nuclear area (pink). Scale bars are 1

µm, except in the zooms 1-5, where they are 250 nm. **(D)** Small arrows point to nuclear bodies. Zooms of areas outlined with white rectangles are shown below without color transparency for clarity. **(E)** Crop of a confocal section (from Fig 2C) stained with phalloidin-AlexaFluor568 (red) and mAb414 (cyan), shown at a similar scale to the TEM images to allow comparison of light and electron microscopic structure.; scale bar is 1 µm. Arrows point to structures possibly corresponding to nucleoplasmic bodies. **(F)** Left: tomogram of a NE spike from a 300-nm thick section of the same oocyte shown in Fig. 3D. Right: model overlay segmented manually to show nuclear membranes and underlying fibrous structures. Scale bars are 200 nm.

Figure 5. NPC conglomerates are internalized while rupture occurs at pore-free regions
(A) Transmission EM images from montage shown in Fig. 3D and colored as in Fig. 4A-D, showing membrane invaginations (left) and nuclear bodies (right). Zooms of portions outlined with white rectangles are shown below without color transparencies. Zoom marked with number 3 is from an area not shown at lower magnification. Scale bars are 1 µm and 500 nm, respectively. **(B)** Tomogram of a nucleoplasmic body (left), with a model overlaid (middle). Right: re-slicing of the volume perpendicular to the view on the left corresponding to the area outlined with an orange dashed rectangle. Scale bars are 200 nm, and 100 nm for image on the right. **(C)** Transmission EM images from montage shown in Fig. 3D and colored as (A) showing rupture. Zooms of the three areas outlined with white squares are shown below. Scale bars are 1 µm and 500 nm for zooms. **(D)** Box plot of distances between neighbor NPCs in different regions and samples. Interphase is an immature oocyte sample; pre-NEBD is a sample fixed a few minutes prior to NE rupture; the other groups come from different regions of the sample shown in Fig. 3C. Measurements were done manually by measuring the length of the line between two NPCs. For more examples of dimples see Fig. S4.

Figure 6. Model of F-actin-driven NE rupture.
Intact NE: interphase organization of nuclear membranes (black lines) with regularly spaced NPCs (yellow cylinders) featuring cytoplasmic filaments and nuclear baskets. Nuclear baskets are embedded in the lamin network (blue filaments). Phase I of NEBD: peripheral NPC components are gradually released, but the NPC core and overall NE structure remains intact. Phase II: NE rupture. First, small patches of F-actin (red) form within the lamina. F-actin patches grow and merge to a shell pushing apart NPCs still partially anchored in the lamina. As frequent F-actin spikes further sever the lamin-to-NE attachments, NPCs segregate into conglomerates leaving stretches of unstable bare membrane, where breaks appear.

Supplemental Material

Supplemental Figure Legends

Supplemental Figure 1. High-resolution TEM montage of a section through the nuclear region of oocyte undergoing NEBD (shown on Fig. 3C). Scale bar 10 µm.

Supplemental Figure 2. High-resolution TEM montage of a section through the nuclear region of oocyte undergoing NEBD, section adjacent to the one shown in Supplemental Figure 1. Scale bar 10 µm.

Supplemental Figure 3. High-resolution TEM montage of a section through the nuclear region of oocyte undergoing NEBD, section from the same oocyte as shown in Supplemental Figure 1. Scale bar 10 µm.

Supplemental Figure 4. Examples of NEBD intermediates classified as dimples.

Shown are crops from sections shown in Figure S2 **(A)** and S3 **(B)**. The crops each show a membrane feature identified as a dimple: a concave NE-membrane portion rich in NPCs. To help orientation, the first crop in each row was pseudo-colored for cytoplasm (green), nucleus (pink) and dimple (orange). Scale bar is 500 nm.

Figure 1.

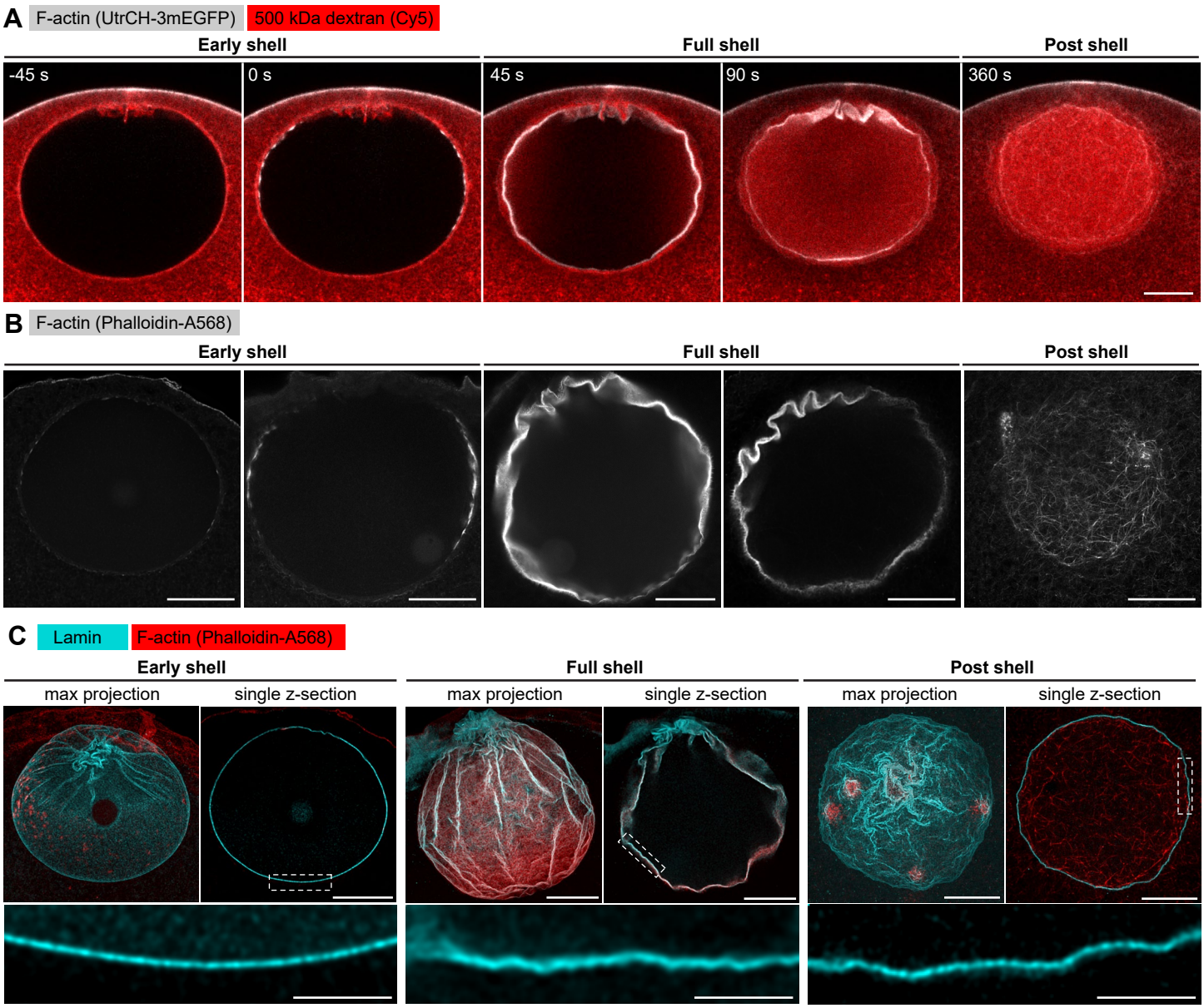

Figure 2.

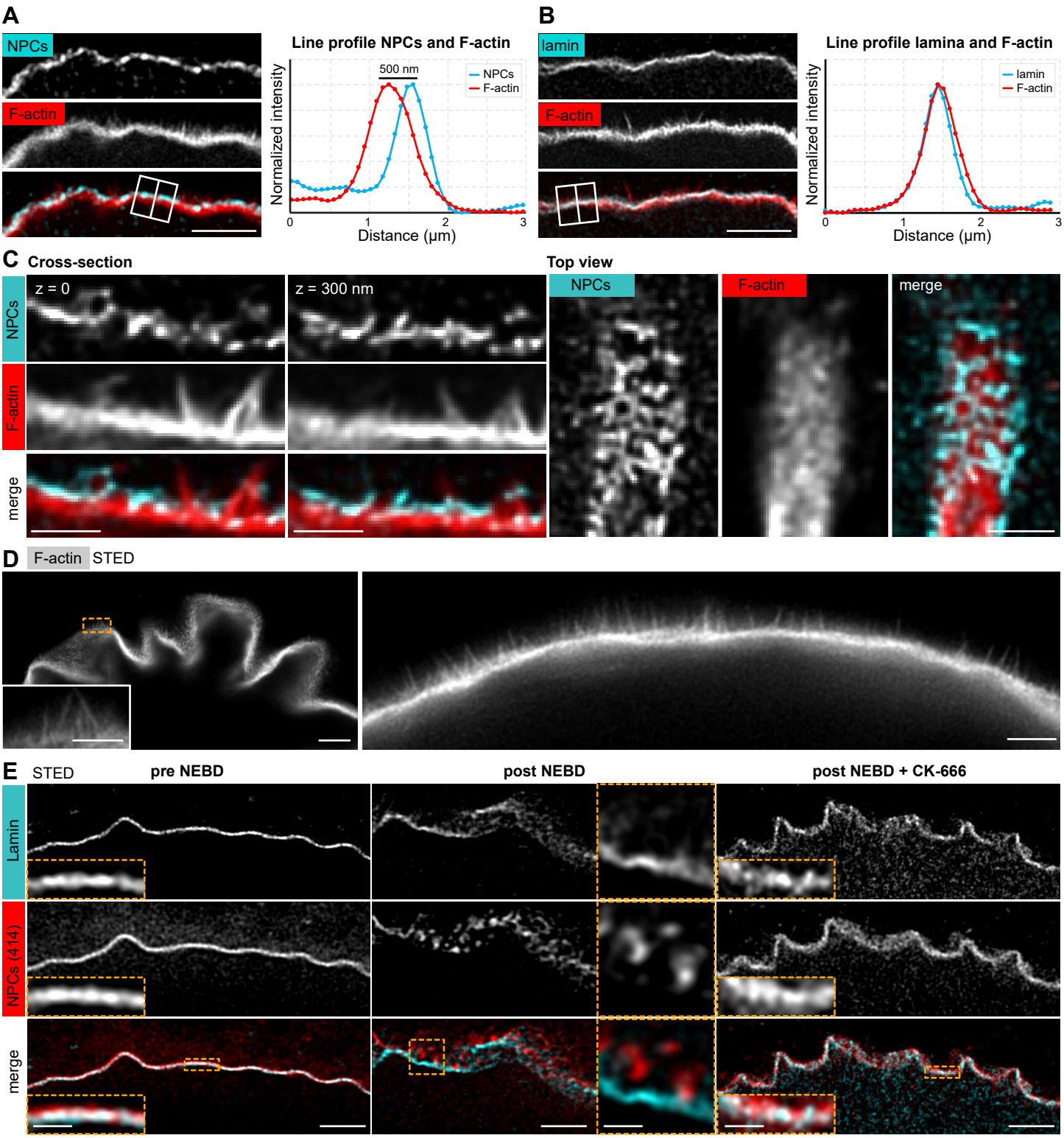

Figure 3.

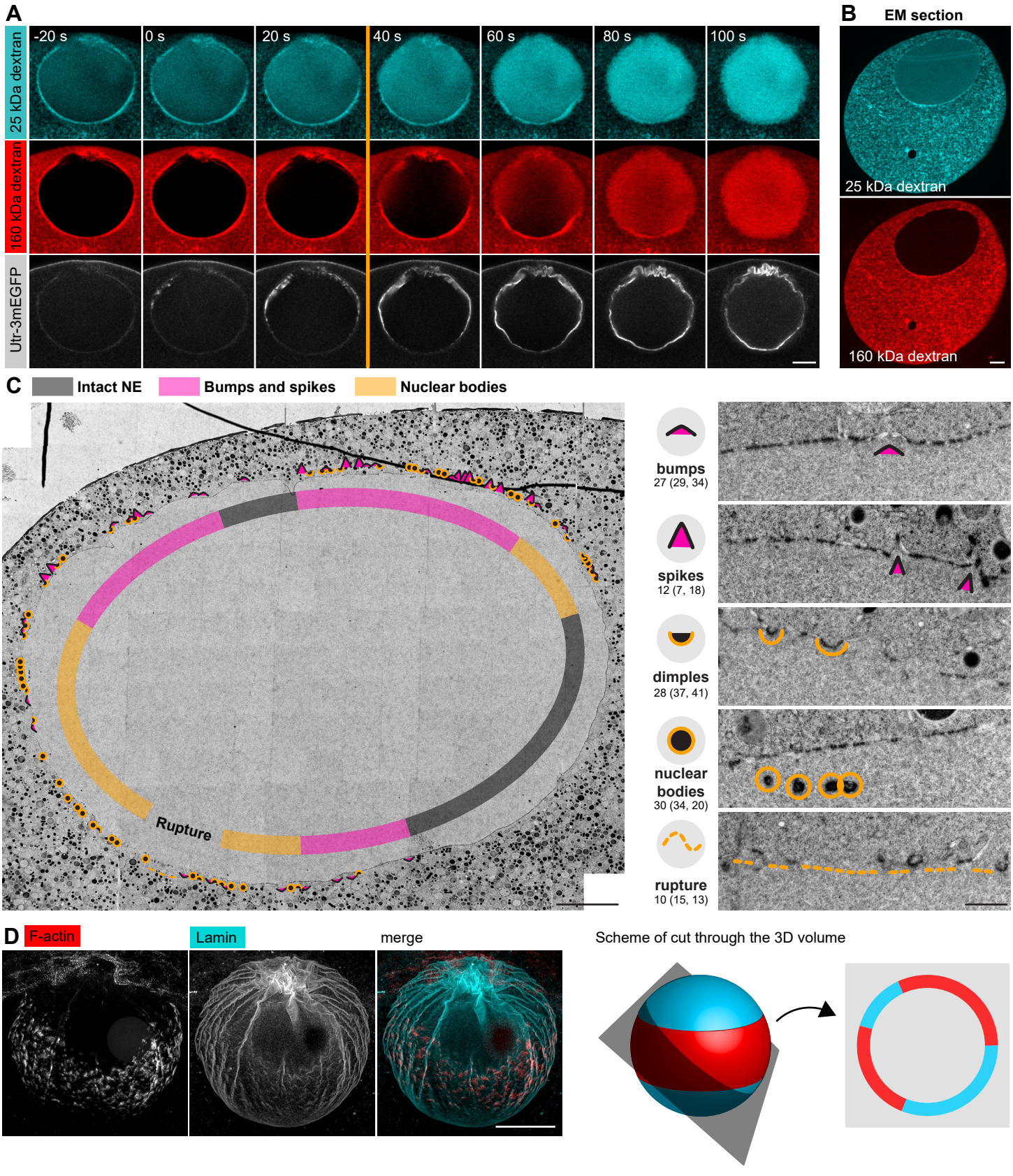

Figure 4.

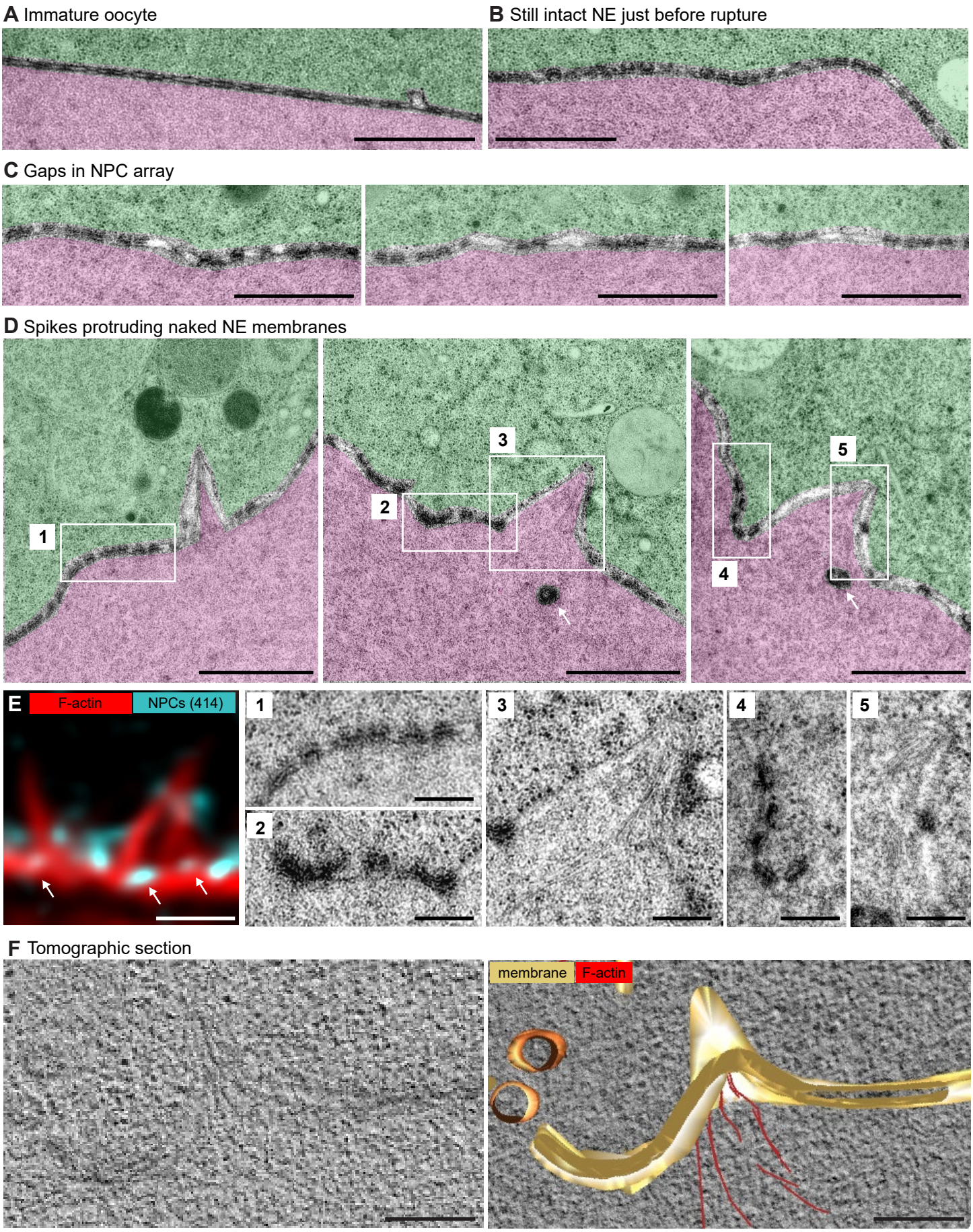

Figure 5.

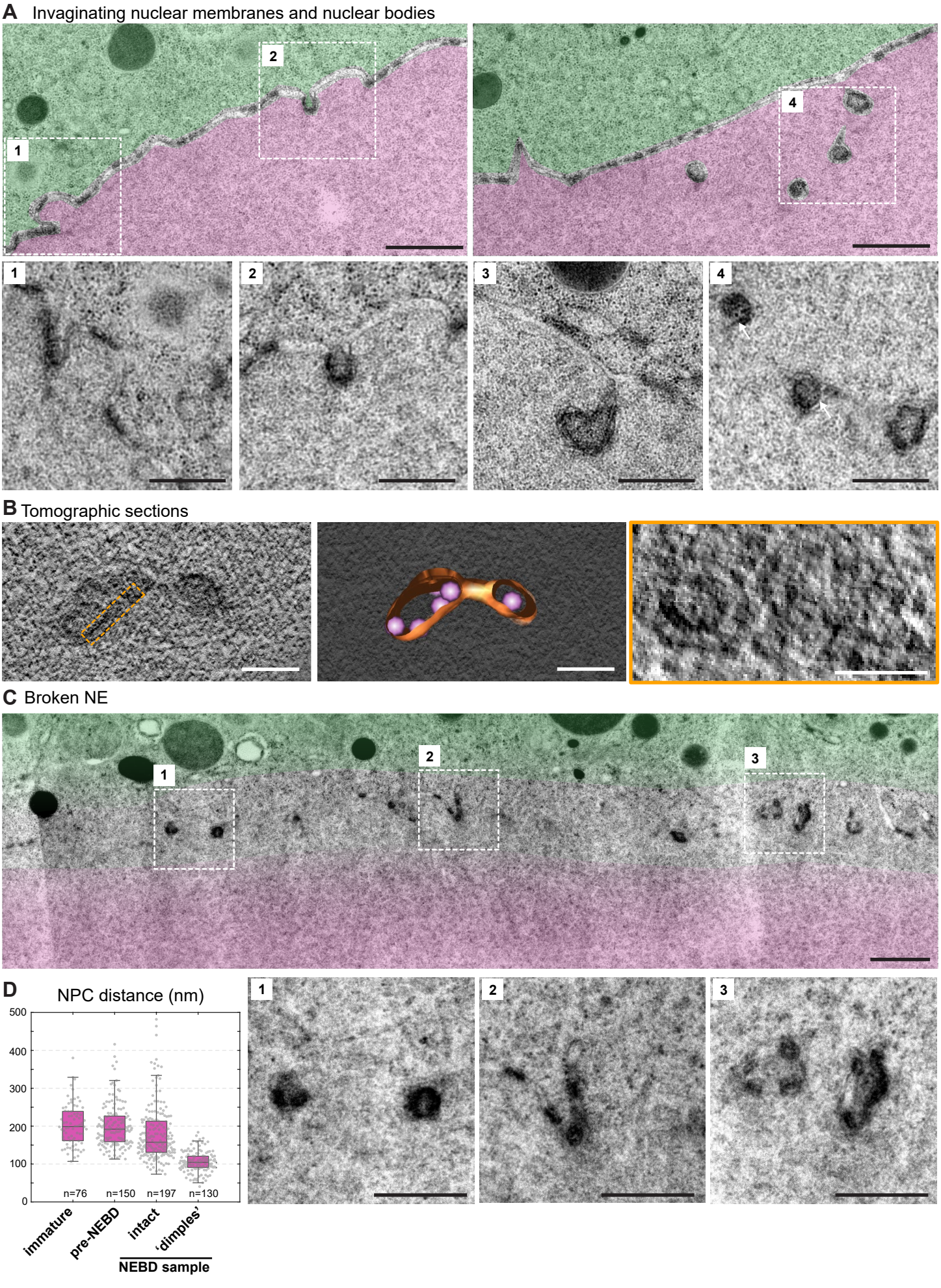

Figure 6.

A